



HAL
open science

Preparation and structural characterisation of model cellular vitreous carbon foams

M. Letellier, A. Szczurek, M.-C. Basso, A. Pizzi, V. Fierro, O. Ferry, A. Celzard

► **To cite this version:**

M. Letellier, A. Szczurek, M.-C. Basso, A. Pizzi, V. Fierro, et al. Preparation and structural characterisation of model cellular vitreous carbon foams. *Carbon*, 2017, 112, pp.208-218. 10.1016/j.carbon.2016.11.017. hal-03101342

HAL Id: hal-03101342

<https://hal.univ-lorraine.fr/hal-03101342>

Submitted on 9 Feb 2022

HAL is a multi-disciplinary open access archive for the deposit and dissemination of scientific research documents, whether they are published or not. The documents may come from teaching and research institutions in France or abroad, or from public or private research centers.

L'archive ouverte pluridisciplinaire **HAL**, est destinée au dépôt et à la diffusion de documents scientifiques de niveau recherche, publiés ou non, émanant des établissements d'enseignement et de recherche français ou étrangers, des laboratoires publics ou privés.

Preparation and structural characterisation of model cellular vitreous carbon foams

M. Letellier¹, A. Szczurek¹, M-C. Basso², A. Pizzi²,
V. Fierro¹, O. Ferry¹, A. Celzard^{1*}

¹ Institut Jean Lamour, UMR CNRS – Université de Lorraine n°7198. ENSTIB, 27 rue
Philippe Séguin, CS 60036, 88026 Epinal cedex, France

² LERMAB, EA Université de Lorraine n°4370. ENSTIB, 27 rue Philippe Séguin, CS 60036,
88026 Epinal cedex, France

* Corresponding author. Tel: + 33 329 29 61 14. Fax: + 33 329 29 61 38. E-mail address :
Alain.Celzard@univ-lorraine.fr (A. Celzard)

Abstract

The aim the present work was to produce carbon foams with as different as possible porous structures but with similar composition and carbon texture for studying precisely the influence of different structural parameters such as density, cell size or interconnectivity on the physical properties of these foams. Over 60 different cellular carbon foams were obtained by pyrolysis of phenolic-furanic rigid foams, whose structure was tailored through some changes in the formulations. The structures of all of these materials were thoroughly characterised through scanning electron microscopy (SEM) and X-Ray microtomography. Both methods proved to give very consistent results, justifying the use of the simpler one, i.e., SEM. Very broad ranges of bulk densities ($0.015 \leq d \leq 0.333 \text{ g cm}^{-3}$) and of average cell diameters ($100 \leq D \leq 5000 \text{ }\mu\text{m}$) were obtained. Despite these very different morphologies, elemental analysis, helium pycnometry and Raman spectroscopy studies showed that the carbon constituting the foams can be considered as identical. The results presented here should be used as a basis for the most thorough and extensive studies of physical properties of vitreous carbon foams.

1. Introduction

Because of their porous nature, rigid foams often offer a good compromise between lightness and performances, hence their growing use in the transportation sector. But beyond lightness, foams can be optimised, depending on the foreseen application, in order to obtain good thermal or acoustic insulators, or shock absorbers for example [1]. Other fields are currently of increasing interest, such as high-temperature insulation, electromagnetic shielding, catalysis or energy conversion [2]. The development of these cutting-edge applications is due to significant progresses in the preparation and characterisation methods of these materials on the one hand, and to the emergence of new functional materials such as ceramics and carbon foams on the other hand.

The present work follows these trends as it deals with the preparation of cellular vitreous carbon foams of controlled structure, thus allowing studying and modelling their physical properties with an unprecedented accuracy. So far, most foams are indeed such that the cell size increases when the bulk density decreases [1], and therefore it has never been possible to definitely attribute some changes of physical properties either to cell size, total porosity or any other parameter. In a former work, decorrelation of cell size and bulk density was approached but was not completely successful [3]. However, the latter pioneering paper opened the route to many new formulations. Most carbon foams presented here were thus derived from thermoset phenolic-furanic polymeric foams. Although similar materials had been produced in the lab since 2009 [4], an extensive formulation and optimisation work allowed for the first time to obtain the amazingly broad range of vitreous carbon foams presented here. As we deal here with model materials having controlled structures, a route is open to the in-depth investigation of the effect of each structure parameter on various physical properties, either validating existing models or suggesting more refined versions, or even evidencing new

phenomena. Doing so, the optimisation of these materials should be possible, depending on the intended field of application.

This type of studies has already been partially attempted in the past, but failed at getting materials of constant composition for which all parameters could be really controlled. Indeed, it has not been possible until now to obtain broad ranges of structures while maintaining everything else constant when using polymeric, ceramic or metal foams. For example, in the polymeric foams investigated by Maheo et al. [5], the material constituting the cell walls was heterogeneous due to a surfactant gradient. In alumina foams, some changes in the microstructure of the struts were observed when the cell size was varied [6]. Regarding metallic foams, their preparation processes limit the diversity of structures, which remains low compared to that of polymeric foams. And finally, the carbon foams existing so far were also difficult to use for this purpose because their manufacturing processes also limited their variability. In this work, organic phenolic-furanic foams of various types were used as precursors which were advantageously converted into cellular carbons made of the same vitreous carbon but with different porous structures.

A precise methodology was adopted here for all cellular foam samples in order to limit the impact of the other experimental parameters and thus to achieve greater repeatability. All these materials were then thoroughly investigated by scanning electron microscopy and X-Ray micro tomography (porous structure), elemental analysis (chemical composition), helium pycnometry (skeletal density) and Raman spectrometry (carbon nanotexture). Based on the data reported here, further works dealing with the influence of precise parameters of the porous structure on the physical properties of carbon foams will be possible.

2. Materials and methods

2.1. Preparation of model cellular carbon foams

2.1.1 Formulations and syntheses

Cellular vitreous carbon foams were produced from phenolic-furanic resins, condensed tannins co-reacted with furfuryl alcohol in the present case, according to the very general route already detailed in [7]. Herein, some refinements and changes in the formulations allowed obtaining the broadest range ever for this kind of materials (see Table 1). The formulations PEG, TRITON PLURO, PMDI and TW were all based on what has been referred to as the “standard” formulation [7], which was called STD when prepared with the specific methodology presented here. These formulations were derived from works reported elsewhere [3,8,9] by addition of various surfactants and plasticisers.

The formulation SF corresponds to tannin-based foam without formaldehyde such as the one presented in [10]. The formulation PPPT corresponds to STD modified by changing the blowing agent from diethyl ether to pentane, adding pMDI as copolymer, Triton X-100 as surfactant and PEG3400 as plasticiser.

T1, T2, T3P, T3DE, T4 and RT were produced by bringing much more significant changes as before to the STD formulation, e.g. mimosa tannin (Fintan OP® kindly supplied by SilvaChimica, St. Michele Mondovi, Italy) was replaced by quebracho tannin (Fintan Q® from the same company) as the main phenolic component. Formaldehyde was replaced by small amounts of glutaraldehyde in T2, T3 and T4 formulations. When diethyl ether was replaced by pentane, more difficult to incorporate into the resin, surfactants were required. Finally, the formulation RT was handled in a different way, by letting it boil for 1h in an oven at 45°C until hardening, thereby leading to a very different pore structure (see below).

A special attention was paid to the repeatability of the precursor organic foams, known to be affected for instance by the type and the size of the mould, the room temperature, etc., and hence a specific experimental protocol was developed. Thus, the ingredients of the present

foaming formulations were carefully mixed in a 2-litres polypropylene box. The latter was next covered with a PVC film and with a non-woven mat of flax fibres wrapped into an aluminium foil (see Fig. 1), and immediately placed in an oven pre-heated at a slightly lower temperature than the boiling point of the blowing agent. Such closed system thermally insulated the mould and retained the heat generated by the reaction, thereby reducing the temperature gradient between the top and the bottom of the foam, and also limited the shrinkage of the materials after foaming. In some cases, however, depending on the formulations, the materials were introduced just after foaming into the oven pre-heated at a higher temperature for accelerating the curing and thus stabilising the foams before they can shrink. Many samples were then cut off the as-obtained big foam blocks for structural and physical characterisation.



Fig. 1. Mould (left) used for the preparation of tannin-based foams (right).

14 types of self-blowing formulations giving foams with different structures were thus produced (see Table 1). The range of available porous structures was further considerably broadened by varying as much as possible the amount of blowing agent. The resultant changes were, however, only possible to a certain extent depending on the formulation, as some materials became inhomogeneous. The structures of only 7 types of formulation, called STD, PEG, PLURO, TRITON, PMDI, T1 and T2, were then varied through the amount of blowing agent.

Table 1. Formulations of the different types of foams.

Type of formulation	Tannin	Furfuryl alcohol	Cross-linking agent	Water	Blowing agent	Plasticiser	Surfactant	PMDI	Catalyst	Foaming temperature
	[g]	[g]	[g]	[g]	[g]	[g]	[g]	[g]	[g]	[°C]
STD	30	10.5	7.4	6	1.5 - 6	-	-	-	11	34
PEG	30	10.5	7.4	6	1 - 6	8 (400)	-	-	11	34
TRITON	30	10.5	7.4	6	1.5 - 6	8 (400)	1.2 (T)	-	11	34
PLURO	30	10.5	7.4	6	1 - 6	8 (400)	1.3 (P7400)	-	11	34
PMDI	30	10.5	7.4	6	1.5 - 6	-	-	-	-	34
T1	30 (Q)	14		9	1 - 7.5	-	1	-	8 (PSA)	34
T2	30 (Q)	14	4.5 (G)	8	5.5 (P)	-	1	-	9 (PTE)	34
T3P	30 (Q)	14	4.5 (G)	9	4.5 (P)	-	1	1.3	8.5 (PSA)	40*
T3DE	30 (Q)	14	4.5 (G)	9	4.5	-	1	1.3	8.5 (PSA)	40*
T4	30 (Q)	28.5	1.1 (G)	-	1.6 (P)	3.8 (EG)	0.6 (P6200) 6.3 (SLES)	-	8.2	100*
TW	30	10.5	7.4	6	5 (P)	12 (400)	1.2 (TW)	-	11	100*
PPPT	30	10.5	7.4	6	4.5 (P)	8 (3400)	1.2 (T)	3.6	11	34
SF	30	21	-	6	3	-	-	-	11	34
RT	30 (Q)	14	-	10	3 (P)	-	0.6 (P6800) 3 (SLES)	-	6 (PTE)	45

*Foaming around 20°C but the foam was quickly put in an oven at the mentioned temperature for hardening and avoiding any shrinkage.

Tannin: Mimosa (Fintan OP®) or
Q = Quebracho (Fintan Q®)

Crosslinking agent: Formaldehyde (37%) or
G = Glutaraldehyde

Blowing agent: Diethyl ether or
P = Pentane

Plasticiser: 400, 3400 = Polyethylene glycol
with molecular weight 400 or 3400
EG = Ethylene glycol

Surfactant: Cremophor ELP® or
SLES = Sodium Lauryl Ether Sulphate
P6200, P6800, P7400 = PLURONIC®
TW = TWEEN 80®

T = TRITON X-100®

Catalyst: paratoluenesulphonic acid at 65% in
water or

PTE = paratoluenesulphonic acid at 65% in
ethylene glycol

PSA = phenolsulphonic acid at 65% in water

2.1.2 Carbonisation of phenolic-furanic foams

All organic foams were then submitted to pyrolysis in the same conditions: heating rate $1^{\circ}\text{C min}^{-1}$ in high-purity nitrogen flowing at 100 mL min^{-1} , final temperature 900°C , dwell time 2 h. Rather high volume shrinkages were observed, from 49 to 65%, from where the need of doing the pyrolysis in a tubular oven of high internal diameter (150 mm) with 3 independently regulated zones. The nature of the carbon obtained after pyrolysis of all formulations is said to be vitreous due to the precursors used here: phenolic-furanic resins, known to lead to this kind of hard carbon. This will be confirmed below by Raman studies.

The thermogravimetric analysis of an STD foam was performed in a STA 449 F3 Jupiter thermobalance (Netzsch) coupled with a QMS 403 C Aëolos mass spectrometer (Netzsch) and equipped with an Oxygen Trap System in zirconium to prevent any oxidation due to the gases released during the carbonisation. The test was carried out in the following conditions: high-purity argon flow 50 mL min^{-1} , heating rate $10^{\circ}\text{C min}^{-1}$ up to 900°C , isotherm of 4 h at 900°C , and two cooling / heating cycles between 200 and 900°C .

2.2. Characterisation

2.2.1 Morphological characterisation with SEM

The most relevant and quantifiable parameters which can be measured on carbon foams such as those shown in Fig. 2 below are bulk density and cell size, objects of the present work. Different window sizes can also be observed, and how they change with density has already been investigated elsewhere [7]. However, the window size may depend on how it was defined, whether it only refers to the open area (i.e., the holes in the cell wall) which is important for transport phenomena, or if it considers all the areas of the cell wall covered with

thinner membranes and which can influence especially the mechanical properties (see for example Fig. 2(d) et 2(e) below). Whatever the definition, the window size is not easily quantified. On the one hand, depending on the accelerating voltage used in the SEM, the thin membranes can indeed be more or less transparent and therefore be totally or partially visible; on the other hand, their measurement requires a large number of images and most of the time automatic measurements are not possible. For these reasons, these parameters will not be reported here.

As the cells of these foams have very different dimensions, it was not possible to analyse them all with the same protocol. SEM images at low magnification were perfect for most materials, but for those having the largest cells (type PMDI), pictures were taken with an optical camera using a precision graduated rule as reference. From a number of images, a method was used based on simple principles of stereology developed by Underwood [11,12]. This method basically consists in counting the number of cells along lines of known length and calculating the corresponding mean linear cell density N_l , see Fig. S1 of the supplementary material. Such count was carried out automatically by application of the ImageJ software¹ on a number of SEM images of each foam sample. The mean linear cell density is the inverse of the mean intercept length \bar{L}_3 , which is related to the average volume V_v and surface S_v of the cells [11-13] according to: $\bar{L}_3 = 4V_v/S_v$. De Hoff [14] showed that the ratio of the average diameter to \bar{L}_3 can be geometrically determined for simple shapes and takes its minimum value of 3/2 in the case of spheres. The cells have been considered perfectly spherical here as already suggested in the work of Gibson & Ashby [1] and in many other publications [15–17]. Their equivalent diameters were then determined as $D = \frac{1.5}{N_l}$. For

¹ <https://imagej.nih.gov/ij>

each material, the cells were counted on a minimum of 8 to 10 lines in each direction, and 3 to 5 images were analysed.

2.2.2 Morphological characterisation with X-ray microtomography

In order to confirm the results obtained by SEM and to quantify as precisely as possible the morphologies of the foams produced here, exhaustive micro-computed tomography (μ -CT) studies were carried out using a Phoenix X-ray Nanotom microtomograph. The principles of tomography were well explained in former works (see e.g. [18–23]) and are not detailed here. Samples for μ -CT had diameters of 7-8 mm and heights of 20 mm. The maximal resolution obtained for these samples was 5 μ m, which is unfortunately not enough to observe all cell walls in these foams. Whereas 3D reconstruction of the samples was rather easy to obtain (see Fig. S2 of the supplementary material), precise morphology quantifications were achieved by application of the Imorph open-source software², which is specialised in foam characterisation in terms of porosity, sizes and shapes of the cells, tortuosity, etc., while having a turnkey approach.

Before any morphological calculation by Imorph, the noise eventually present in the images was removed through successive erosion and dilatation operations. The region of interest (*ROI*) was chosen as a parallelepiped fully included and centred in the foam to avoid any edge effect. In order to separate the porosity from the solid phase, a threshold value was determined by Otsu's method [24] in Aphelion® software³. This method calculates, without any subjective choice from the operator, the optimum threshold separating the two phases so that their intra-class variance is minimal. Such method was repeatable and comparable for all

² <http://imorph.sourceforge.net>

³ www.adcis.net

foams. The cells sizes and shapes were then determined in Imorph using granulometric operations followed by the segmentation of the cells with a watershed based on the maximal balls method (see [25] for details). This method allowed segmenting precisely the cells and providing quantitative information about the dimensions and the shapes of the corresponding ellipsoids as well as the diameters of the spheres of equivalent volumes.

In order to optimise accuracy and calculation time, a sensitivity study was performed based on 3 parameters: resolution, sample size (i.e., number of 2D images) and granulometric error (used in Imorph to accelerate the calculations). When the resolution was decreased from 5 to 10 and 15 μm , the measured cells size increased because of an incorrect segmentation of the cells (see Fig. S3(a) of the supplementary material). However, the values converged quickly when the resolution increased so that the resolution of 5 μm used here had no significant impact on the cells diameters. The number of 2D images used for the 3D reconstruction was varied from 1000, 800, 600, 400 to 200 (see Fig. S3(b) of the supplementary material). The average cell diameter decreased with the sample size, as the biggest cells were less and less fully included and then taken into account. At least 600 images were required for an STD foam with an average cell diameter of 390 μm . It was then decided to use the maximal number of images (1000) for all foams. The granulometric error was increased from 0, 0.5 to 1 without notable change (see Fig. S3(c) of the supplementary material). However, it was kept constant at 0.5 to avoid any influence for other samples.

2.2.3 *Elemental analysis*

Elemental analysis was performed here along with pycnometry and Raman spectroscopy to check that the carbon from which the foams are made is the same and hence to be sure that the observed differences of physical properties are only due to some differences of porous structures. Two to three samples belonging to the most different formulations, i.e., 11 out of

14: STD, PEG, TRITON, PMDI, T1, T3, SF, PPPT, RT, TRF, and TFA, were analysed. The contents of C, H, N and S were measured in an elemental analyser Vario EL Cube (Elementar) through the combustion of samples in a quartz tube at 1150°C under helium and oxygen in excess. The oxygen content was estimated by difference.

2.2.4 *Skeletal density of carbon foams*

The skeletal density of the carbon constituting the foams, ρ_s (g cm^{-3}), is a very important data for calculating accurately the relative density of the foams d_r (dimensionless), the latter being used as a reference for comparing different foams in this project. The skeletal densities of not all carbon foam samples of the present work were measured, but those of STD and PEG formulations which led to the most different carbon contents (see next section), using an automatic helium pycnometer AccuPyc 1340 (Micromeritics, USA). The samples were ground into fine powder to be able to introduce as high amounts of material as possible in the sample holder, but also to limit the contribution of any possible closed porosity. These powders were also dried overnight at 120°C under vacuum to avoid any influence of humidity on the results. Finally, measurements were carried out at 30°C for preventing as much as possible any helium adsorption phenomenon. These measurements of skeletal density were fast due to the complete absence of narrow porosity in the corresponding vitreous carbon. Indeed, the BET surface area measured for a number of samples and not reported here was also within the limit of accuracy of the adsorption device, i.e., far below $1 \text{ m}^2 \text{ g}^{-1}$. Such order of magnitude was already reported elsewhere for standard tannin-based carbon foams [4,7].

2.2.5 *Raman studies*

Raman spectroscopy studies were carried out with a spectrometer Horiba XploRA without special sample preparation. The spectra were collected under a microscope using a $\times 100$ objective. The signal from Raman scattering was dispersed by a holographic grating with

1200 lines per mm and detected by a CCD sensor. A laser with a wavelength of 532 nm and filtered at 1% of its nominal power was used. It has been carefully checked through some repeated measurements at the same sample spot that the corresponding incident power of about 0.14 mW was low enough to prevent overheating and / or sample degradation. For each spectrum, two accumulations from 50 to 4000 cm^{-1} with an integration time of 120 s were done. It was systematically checked that no significant difference was observed when the analysis was performed in different areas of the same sample, especially when the surfaces of cells and those of broken struts were compared. In the following, only one out of at least 3 spectra obtained at different zones of samples of each kind was therefore given and compared with each other.

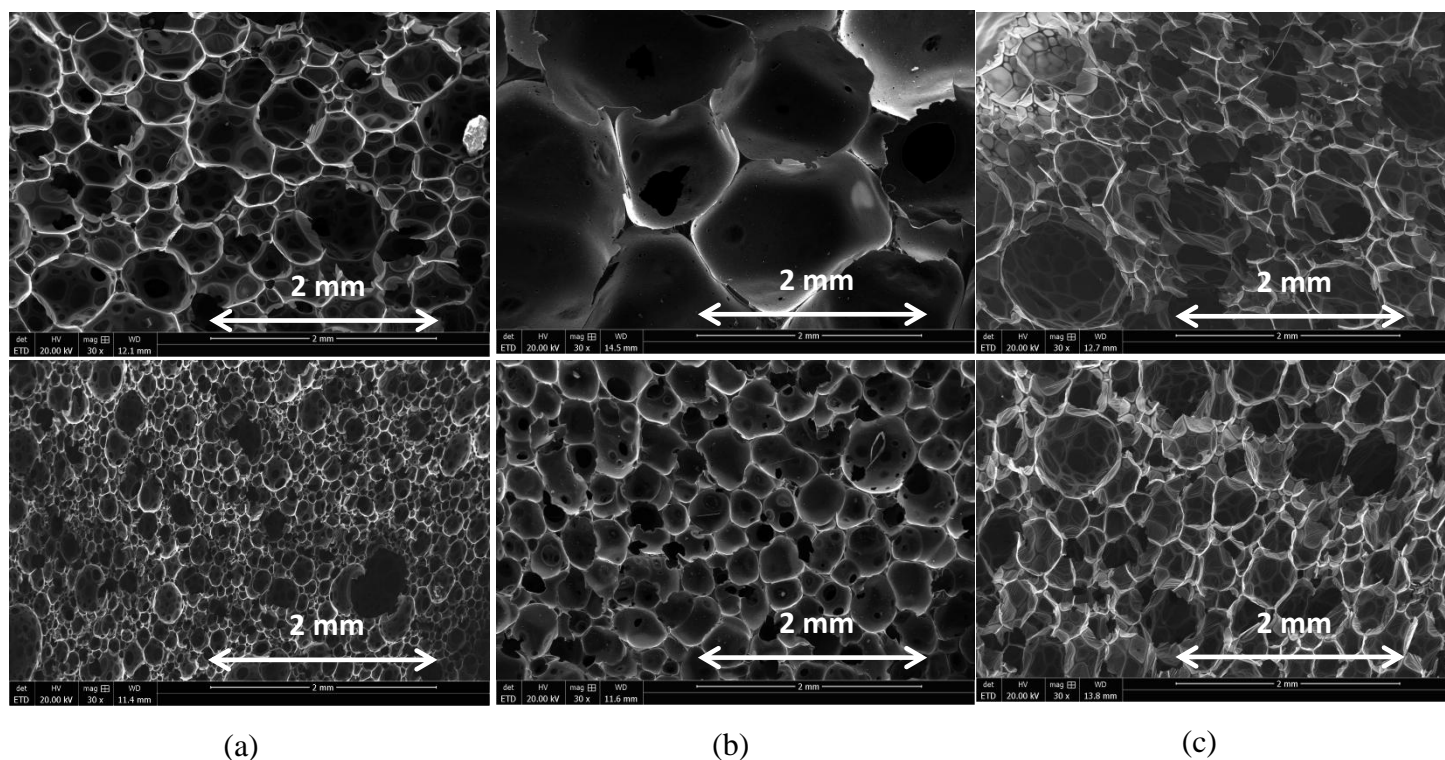
3. Results and discussion

3.1. General morphological features of phenolic-furanic foams

The impact of the formulations given in Table 1 on the morphology of carbon foams is discussed below and, for that purpose, representative examples are presented in Fig. 2 and in Fig. S4 of the supplementary material. PEG, TRITON PLURO, PMDI and TW foams (see one example in Fig. 2(b)) were relatively close to each other as their formulations were close to that of STD (Fig. 2(a)). Especially, PEG, TRITON and PLURO had different ranges of density and cell sizes than those of STD (see Fig. S4), which is an extremely important feature in the context of the present studies. PMDI and PPPT foams were also comparable but with thicker walls, those of PPPT being porous. PPPT (Fig. 2(f)) was indeed formulated in order to obtain carbon foam having simultaneously large cells and thick cell walls. This objective was achieved by the presence of pMDI and PEG3400 or rather high viscosity. With such formulation, the foams had much thicker cell walls but slightly lower average cell sizes than those of the PMDI formulation.

T1, T2, T3P, T3DE, T4 and RT (see some examples in Fig. 2(c) to Fig. 2(f) and other SEM images provided in Fig. S4 of the electronic supplementary information) were very different from STD, due to their significant different formulations explained in subsection 2.1.1. Thus, their low contents of crosslinker were balanced by the use of more furfuryl alcohol, of pMDI (for T3) and of phenolsulphonic acid. This allowed obtaining a very fast hardening of the foams and then a negligible shrinkage. The decrease of the amount of water and its substitution by ethylene glycol also led to better heat transfer throughout the materials and then to more homogeneous foams.

The cell walls in carbon foams T1 to T4, SF and TW were very thin and less perforated than in STD, but they showed some wrinkles and looked like torn in some places (see Fig. 2(d)). These features illustrate the difficulty of quantifying windows sizes. Finally, as explained before, RT was the only tannin-based foam having a truly reticulated structure, i.e., without cell walls, and is therefore the exception in this series of cellular carbon foams (see bottom of Fig. 2(f)).



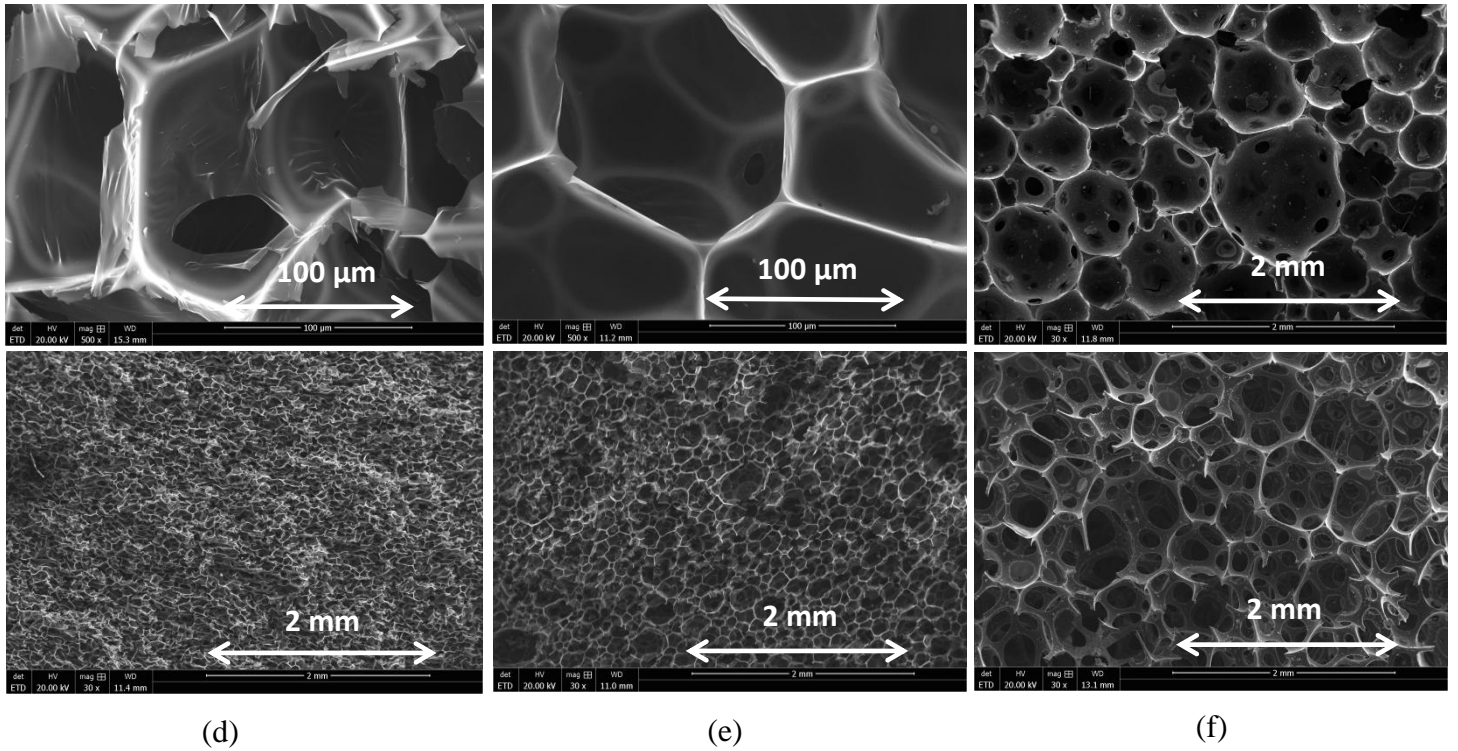


Fig. 2. SEM pictures (secondary electrons detector) of vitreous carbon foams prepared from different formulations (see text): (a) type STD ($\times 30$) with densities of 0.043 (top) and 0.111 g cm^{-3} (bottom); (b) type PMDI ($\times 30$) with densities of 0.091 (top) and 0.188 g cm^{-3} (bottom); (c) type T1 ($\times 30$) with densities of 0.021 (top) and 0.033 g cm^{-3} (bottom); (d) type T2 with densities of 0.050 ($\times 500$, top) and 0.129 g cm^{-3} ($\times 30$, bottom); (e) types T3P ($\times 500$, top) and TW ($\times 30$, bottom) with densities of 0.036 and 0.044 g cm^{-3} , respectively; (f) types PPPT ($\times 30$, top) and RT ($\times 30$, bottom) with densities of 0.094 and 0.043 g cm^{-3} , respectively.

Carbon foams T1 to T4, as well as SF and TW, had lower densities, less than 0.05 g cm^{-3} , than those derived from other formulations. Especially, the high amounts of furfuryl alcohol and surfactants in T4 led to the lightest tannin-based foam ever produced with a bulk density of 0.01 g cm^{-3} . Even by dramatically reducing the amount of blowing agent in T1 to T3, those carbon foams had densities never higher than 0.05 g cm^{-3} .

The ranges of bulk density that could be achieved by playing with the amount of blowing agent also strongly depended on the type of formulation, see Fig. 3. For instance, the foams of types PEG, TRITON and PLURO presented bulk densities inversely proportional to the amount of blowing agent, similarly to what has been experimentally evidenced and theoretically demonstrated elsewhere [7]. But the formulations STD, PMDI and T1 followed power laws with exponents - 0.77, - 0.71 and - 0.70, respectively. As it was not possible to vary the quantity of blowing agent of T2 without decreasing drastically its homogeneity, samples with various densities were cut off different homogeneous blocks.

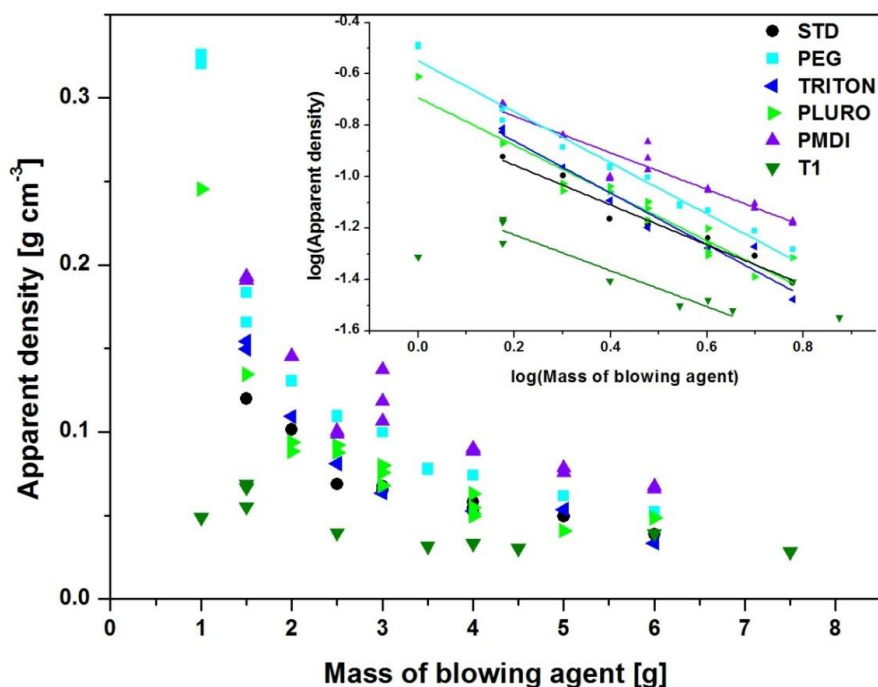


Fig. 3. Changes of bulk density of cellular carbon foams as a function of the amount of blowing agent (diethyl ether) in the initial formulation. Power law fits to the data of each type of formulation are shown in the inset.

3.2. Carbonisation of phenolic-furanic foams

The mass loss after pyrolysis ranged from 52 to 68%, depending on the formulation. The thermogravimetric analysis of the STD foam performed in the thermobalance as explained in subsection 2.1.2 is presented in Fig. 4.

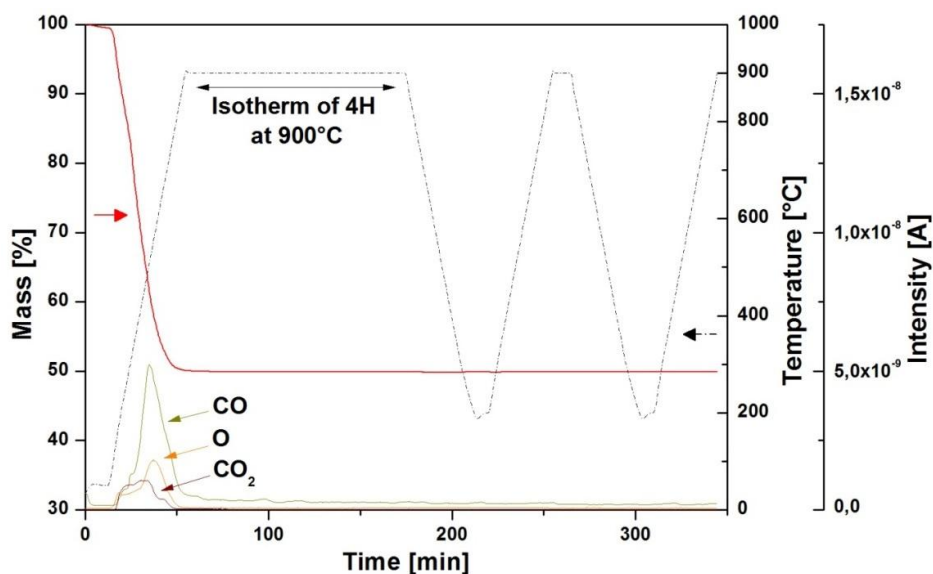


Fig. 4. Thermogravimetric analysis of an STD organic foam and simultaneous mass spectrometer analysis of the emission of CO, O and CO₂ as a function of time. After the pyrolysis up to 900°C, one 4h-long isothermal segment of and two other cycles of heating and cooling between 200 and 900°C were performed. The data from the detector of the mass spectrometer are in Ampere (no calibration).

It was found that the foam lost some mass only during the first heating step up to 900°C, during which various gases were released: organic compounds with high m/z ratios (not shown in Fig. 4), water (H₂O and HO with $m/z = 18$ and 17 , respectively, not shown), and CO₂ ($m/z = 44$), CO ($m/z = 28$) and O ($m/z = 16$). After the sample reached 900°C, the mass spectrometer did not detect gases anymore, and no further mass loss was measured by the thermobalance. Both cooling and heating cycles that followed confirmed the stability of the carbon foams up to the final carbonisation temperature of 900°C.

For all materials, the mass loss was slightly higher or equal to the volume shrinkage. The resultant bulk densities of the carbon foams were therefore slightly below or approximately equal to those of the organic foams, see Fig. 5. The carbon foams T1 and T4 exhibited higher

mass losses and lower shrinkages, thus their densities were the most different from those of the starting organic foams. However, these changes of density remained quite low, and the strong similarity between the densities of carbon and organic foams facilitated the preparation of carbon foams with controlled densities.

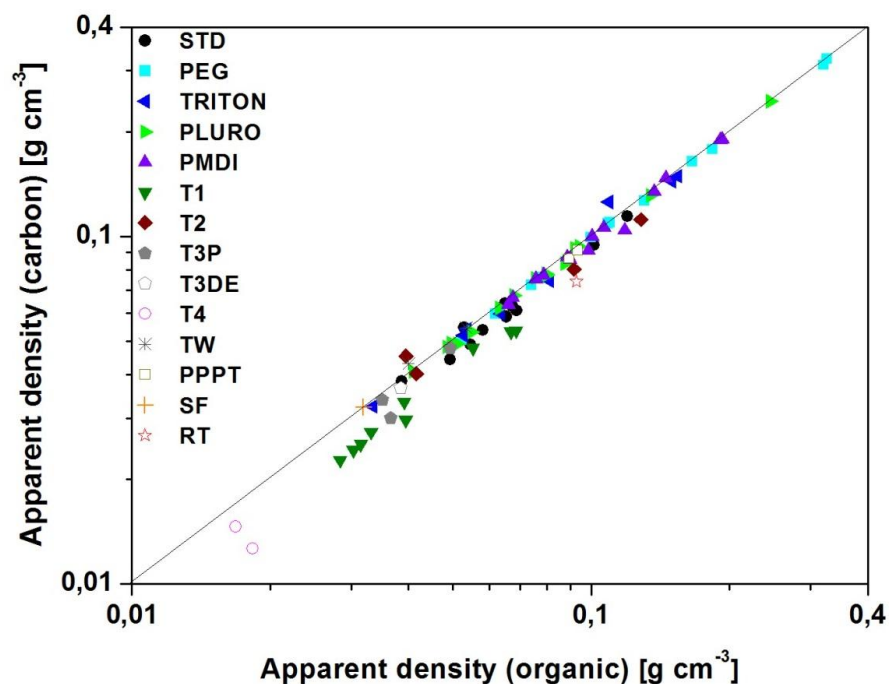


Fig. 5. Comparison of the bulk densities of foams made from different formulations, before and after pyrolysis.

3.3. Studies of the vitreous carbon

The results of elemental analysis are given in Table 2. All the carbon foams, except T4, presented C contents ranging from 89% to 94%, i.e., with an average level of $91.5 \pm 2.5\%$. This uncertainty is typical for this kind of analysis, and suggests that these differences are not really significant. The differences observed between samples in terms of H and S contents were not significant either. However, N contents of PMDI, PPPT foams were slightly higher. These differences are easily explained by the presence of isocyanates in PMDI and PPPT formulations. T4 foam seemed to have a composition slightly different from the others with

higher oxygen content. This is explained by the higher amount of furfuryl alcohol used in its formulation. However, T4 was so lightweight and fragile that its handling was too difficult for most characterisations, thereby preventing any further investigation of its physical properties.

Table 2. Elemental analysis of carbon foams. All elements are expressed in wt. %.

Formulation	N	C	H	S	O*
STD	0.7	90.5	0.7	1.2	6.9
PEG	0.6	93.7	0.6	0.4	4.7
PLURO	0.4	90.7	1.3	0.4	7.1
TRITON	0.7	93.2	0.6	0.5	5.0
PMDI	1.3	92.2	0.7	1.0	4.7
T1	0.4	91.6	0.6	0.4	6.9
T2	0.3	89.6	1.5	0.8	7.7
T3	0.5	89.5	0.7	0.2	9.0
T4	0.2	86.9	1.7	0.6	10.7
TW	0.4	89.0	1.8	0.7	8.1
SF	0.7	90.9	1.2	0.9	6.4
PPPT	1.1	92.5	1.5	0.7	4.2
RT	3.7	88.8	1.2	1.1	8.2

* Estimated by difference

The very similar results of elemental analysis presented above suggested that similar skeletal densities had to be expected. One STD foam was analysed using the highest possible mass that could be introduced in the pycnometer (near 2.3 g), and a density of 1.976 g cm^{-3} was measured. Three samples of a PEG foam were analysed and a resultant skeletal density of $1.976 \pm 0.007 \text{ g cm}^{-3}$ was also found. A value of 1.98 g cm^{-3} was also formerly reported for carbon foams derived from standard formulation of tannin-based foams [4,7]. A higher value of 2.03 g cm^{-3} [3] was found for other tannin-based foams where pMDI was used, but this

difference was not significant because of the larger standard deviation of $\pm 0.11 \text{ g cm}^{-3}$. This value of 1.98 g cm^{-3} therefore seems to be appropriate for a large number of carbon foams derived from tannin as confirmed by the value of $1.98 \pm 0.02 \text{ g cm}^{-3}$ again determined for "carbon meringues", also derived from a similar formulation containing tannin [16]. Such values are rather high compared to the skeletal density of commercial vitreous carbon foams: 1.538 g cm^{-3} for Ultramet RVC⁴, or of glassy carbon: 1.51 g cm^{-3} for Tokai Carbon⁵ and 1.42 to 1.54 g cm^{-3} for HTW⁶ (depending on the final temperature of carbonisation, 3000 and 1000°C , respectively). This difference may be first explained by the higher purity of the carbon claimed by these producers which are always well above 99% . The final temperature of carbonisation of the present tannin-based foams are also lower than those of the commercial foams, which may explain the higher proportions of heteroatoms (of higher atomic weights than carbon), and the different carbon texture. Furthermore, industrial processes are highly controlled and allow obtaining high purity especially in terms of metal contents, which can be largely removed by pyrolysis up to 3000°C . Additionally, tannin is a raw material containing a few inorganic impurities, as highlighted by the X-ray diffraction pattern of a standard carbon foam presented elsewhere [4]. Finally, for RVC foams and industrial vitreous carbon, the heating rate is known to have a great influence on the density of the final carbon and can provide skeletal densities as low as 1.06 - 1.27 g cm^{-3} for glassy carbons heated up to 3000°C [26]. As a conclusion, as the chemical compositions of STD and PEG formulation were the most "different" from the STD, and that the value of 1.98 g cm^{-3} was already found for all other types of tannin-based carbon foams, it was then decided to use this value of 1.98 g cm^{-3} for all the carbon foams produced here.

⁴ <http://www.ultramet.com>

⁵ <http://www.glassycarbonstore.com>

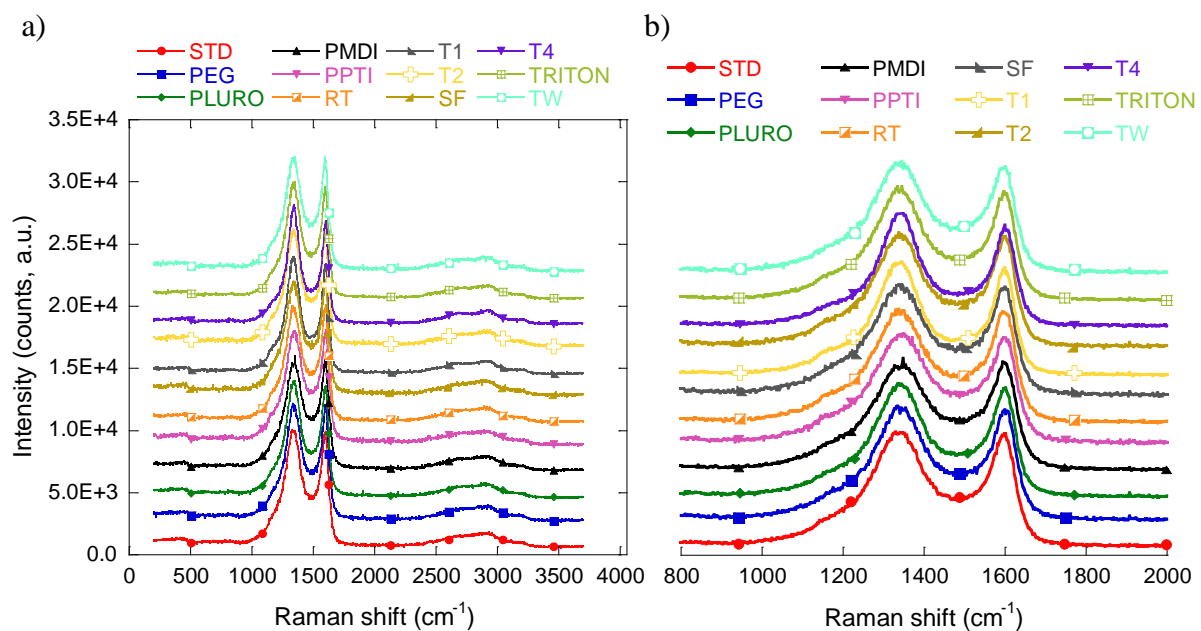
⁶ <http://www.htw-germany.com>

The Raman spectra of an STD carbon foam used as reference were obtained from various zones of a given sample. 3 spots corresponding to broken struts on the one hand, and 3 spots corresponding to smooth cell surfaces on the other hand were investigated at a wavelength of 532 nm, and the resultant spectra are given in Fig. S5 of the supplementary material. The intensity ratios of D/G bands were 1.016, 1.020 and 1.018 for struts, and 1.010, 1.016 and 1.034 for cells surfaces, i.e., the average D/G ratios were 1.018 and 1.020 for struts and cells. As no differences in the positions of D and G bands could be seen either ($1344 \pm 5 \text{ cm}^{-1}$ and $1598 \pm 3 \text{ cm}^{-1}$ for D and G, respectively), it can be concluded that there is no significant differences of carbon texture at the sample surface and beneath the surface. This finding is rather logical as far as vitreous carbon is concerned, whose highly disordered nature is confirmed by the general shape of the Raman spectra. The broad D band and the slightly narrower G band of rather similar intensity, combined with the shallow valley between them and the shoulder at around 1200 cm^{-1} (accounted by contributions called D3 and D4, respectively), are indeed typical of such shiny and brittle carbon, presenting a conchoidal fracture with sharp edges like glass. D4 is said to be related to a poor organisation of carbon, and D3 also appears when the crystallisation degree is very low [27]. In contrast, graphitisable foams present different carbon ordering at the outer surface with respect to the bulk of the struts, and hence different D/G ratios, due to the different stretching-induced orientation of the material during the formation of the foam [28]. Such effect could never be observed here.

As the carbon from which the foams are made was obtained by pyrolysis at 900°C of phenolic-furanic formulations, recovering vitreous carbon was expected and was at least partly evidenced by the brittle, smooth, solid and shiny character of the material. Raman spectra further confirmed the vitreous nature of the carbon as the positions of D and G bands, their general shapes and their FWHM values fully match those already reported for glassy

carbon derived from phenolic resins or from polyfurfuryl alcohol pyrolysed below 1000°C (see for instance [29-33]).

The raw spectra of the most important carbon foams series (one sample for each formulation at 532 nm) are gathered in Fig. 6(a). All were extremely similar at both 1st and 2nd orders, and the zoom on the 1st order shown in Fig. 6(b) further confirms this finding. The D/G intensity ratios are given in Fig. 6(c), wherein the position of the corresponding bands is also shown. D/G ratios are all included in a range of values very similar to the data scattering observed with the STD foam alone, with an average value of 1.020 ± 0.015 . Such low ratios correspond to quite small distance L_D between structural defects and correspond to a zone in the plot of D/G ratio versus L_D where the corresponding curve is almost vertical. In other words, I/D values ranging from 1 to 1.5 can be obtained at very similar values of L_D [34]. The positions of the maxima of the bands are also all very similar, and no trend appeared when plotted as a function of the D/G ratio. The aforementioned considerations all tend to conclude that the nanotexture of the carbon from which all these foams are based on is nearly the same, and therefore the physical properties to be investigated in future works are only related to some changes of porous structure.



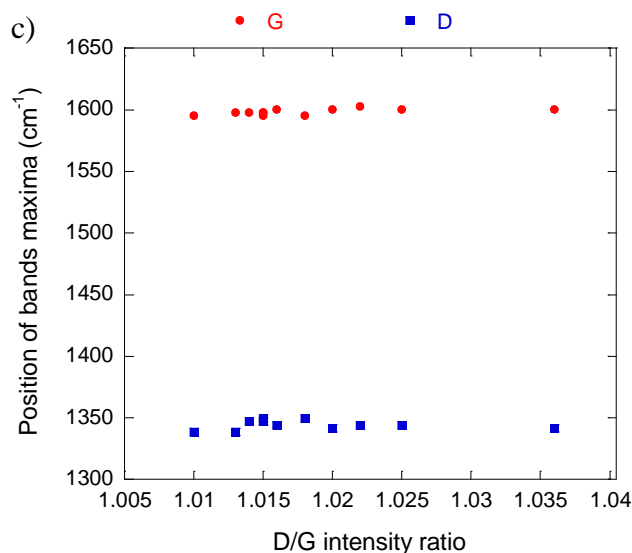


Fig. 6. Raman spectra at 532 nm of most carbon foams presented in this study: (a) full spectra; (b) zoom on the 1st order part; (c) positions of D and G bands as a function of D/G intensity ratio.

Fig. S6 of the supplementary material presents the positions and the full width at half maximum (FWHM) of D and G bands, compared to the many data collected by Beyssac et al. [35] for disordered and heterogeneous carbonaceous materials. The present Raman data were not obtained at the same wavelength (532 nm) as in [35] (514.5 nm), but this only affects the position of the D band by a little shift towards lower wavenumbers. Apart from that, our data correspond to highly disordered carbon as proved by the rather high FWHM of their G band. FWHM in the range of $62.3 \pm 3.5 \text{ cm}^{-1}$ indeed correspond to quite low crystallite size, around 3 nm [36] or below 2.8 nm as reported elsewhere [37]. The latter paper also suggests that the experimental scattering in such a range of FWHM values doesn't allow separating the samples or assuming that one has a truly more ordered nanotexture than another. As already suggested by elemental analysis, T4 was the only one being a little different. Although its G band was exactly in the same range of width of all other foams, 63 cm^{-1} , its D band was indeed narrower with a width of 114 cm^{-1} , against an average and standard deviation of 140

cm^{-1} and 7 cm^{-1} , respectively, for the rest of the materials. However, as already explained above, this material was too brittle for further tests and will not be considered further.

3.4. Critical morphological analysis

The average cell diameters D determined by SEM are shown in Fig. 7 as a function of bulk density ρ for the different types of formulation. Power laws such as $D = A\rho^x$ were suggested elsewhere [7], where A and x are constants depending on the type of foams studied. This equation was indeed appropriately fitted to the experimental data, and the corresponding values of A and x are listed in Table 3. These fits are of great importance for further studies, especially for the characterisations of foams' physical properties. They indeed allowed calculating the average cell sizes of any sample whose density was in the range investigated here, instead of performing a tremendous amount of measurements which would have not been technically possible. Fig. 7 clearly shows that a major objective of this work was achieved, as it demonstrates the possibility of having at our disposal carbon foams having one given cell diameter but very different porosities, or a broad range of cell sizes (up to more than one order of magnitude) at a given porosity. This major feature is clearly evidenced by drawing either horizontal or vertical straight lines, respectively, at different positions across the linear fits presented in Fig. 7.

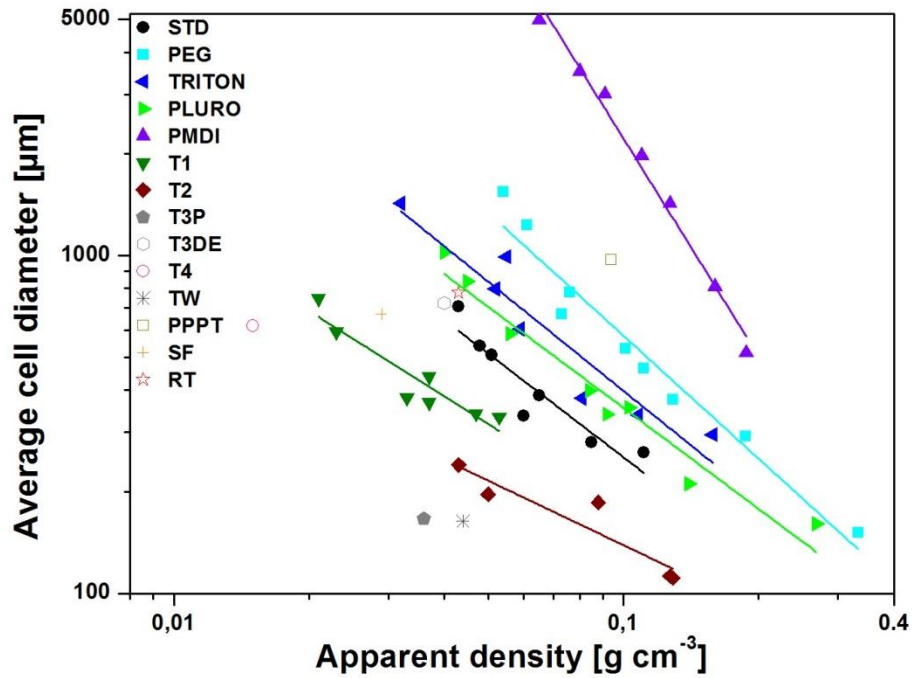


Fig. 7. Average cell diameter determined from SEM pictures as a function of bulk density. The straight lines are power law fits such as $D = A\rho^x$ to the data sets of each type of formulation.

Table 3. Adjustable coefficients of the power law fits to the data of Fig. 7.

	STD	PEG	TRITON	PLURO	PMDI	T1	T2
A	24.2242	35.7874	33.6008	35.9335	15.9919	25.7199	32.23629
x	-1.01964	-1.2101	-1.07404	-0.99422	-2.14407	-0.83926	-0.63497

Three geometrical parameters of the cells were determined here from μ -CT: average equivalent diameter, distribution of cells diameters, and sphericity. In Fig. 8, the cells diameter of an STD foam of density 0.065 g cm^{-3} are presented as histograms and cumulated percentages. These distributions change whether they are based on the number of cells (Fig. 8(a)) or on the volume filled by these cells (Fig. 8(b)), for each class of diameters. The diameters were correctly accounted for by log-normal distributions (see Fig. 8). This finding

is not surprising because natural phenomena are often multiplicative with asymmetric data and hence are well described by log-normal distributions [38]; this is especially relevant for morphological characterisations as already observed elsewhere [39,40].

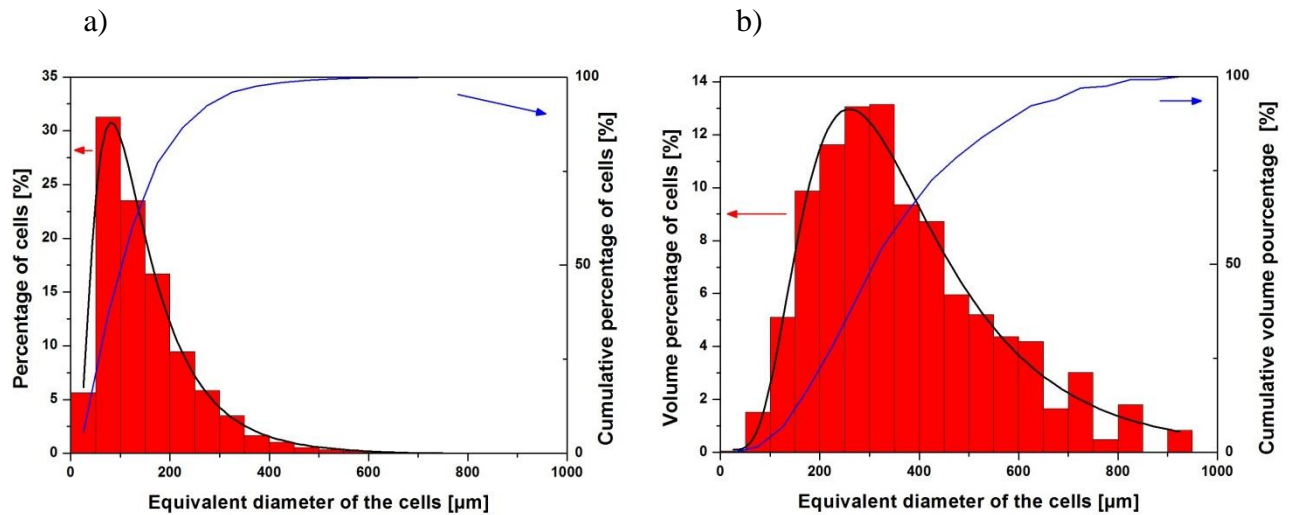


Fig. 8. Number-weighted (a) and volume-weighted (b) distributions of equivalent cell diameters of an STD foam sample of bulk density 0.065 g cm^{-3} . The curves corresponding to the cumulative percentages and to log-normal fits of the distributions are also shown.

It was not possible to analyse all the foams produced here because of the corresponding huge amount of data and calculation time required. However, 36 different foams corresponding to almost all the present formulations, and involving more than 1 To of data, were analysed. The corresponding cells sizes are presented in Fig. 9 in terms of geometric mean and standard deviation derived from the log-normal fits. As already observed in Fig. 8, the number-weighted equivalent diameters are far smaller than the volume-weighted ones. This finding suggests that all the foams contain a lot of small cells (with equivalent diameters below $200 \mu\text{m}$) but which represent only a low fraction of the total porosity. The biggest cells have major influence on the porosity and then on the transport phenomena. The use of

volume-weighted diameters is also more relevant when describing foams as periodic repetitions of unit cells, many small cells being only at the junction of bigger ones. Hereinafter, only the volume-weighted diameters were thus investigated in detail, and indeed found to be similar to the values obtained by SEM analysis (see below).

The polydispersity indexes P_{index} were calculated from the histograms of cell diameters according to [23,41]. These indexes range from 0 and 1, the value 1 meaning that the distribution is monodisperse. For the cellular foams, number-weighted distributions produced values of P_{index} which decreased when the average cell size increased, whereas volume-weighted distributions led to roughly constant P_{index} values around 0.9, see Fig. 9(a). The latter corresponds to rather narrow and similar dispersions of cell sizes for all foams. In order to look deeper at the homogeneity of these foams, the confidence intervals containing 68% of the cells diameters were compared in Fig. 9(b). In a general way, these intervals increased with the average cell sizes. The least monodisperse foams were the formulations types RT, PLURO, T1, T2 and STD, by decreasing order of homogeneity. TW and T3P foams were the most monodisperse.

Finally, the average sphericity index was calculated, defined as the ratio of minor to major axes of the cells considered as ellipsoids of revolution. Fig. 9(c) shows that most foams had rather spherical cells as their sphericity indexes ranged from 0.8 and 0.9. Some materials presented lower sphericity but this might be due to the too low resolution of the tomograph, which limited the segmentation of neighbouring cells. It can be concluded that the produced carbon foams present slightly elongated but repeatable cells, leading to a low and similar anisotropy for all materials.

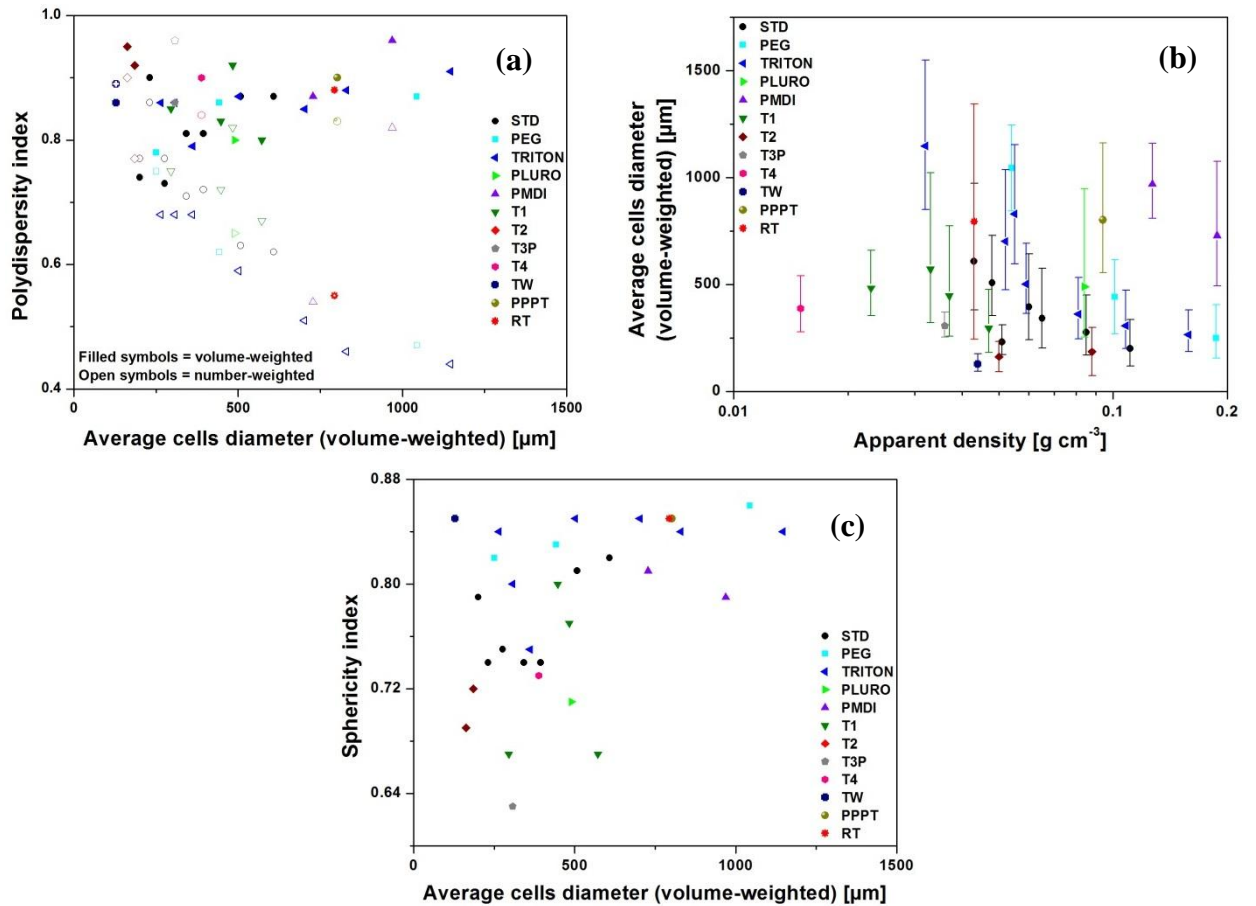


Fig. 9. (a) Polydispersity indexes of number-weighted and volume-weighted distributions; (b) volume-weighted average cell diameters, with their 68% confidence intervals, as a function of bulk density; (c) sphericity indexes as a function of average cell diameter.

The thorough analysis of many carbon foams by μ -CT in order to get a precise knowledge of cells characteristics required quite expensive equipment and was time-consuming, not only for acquisition but also for data treatment. In contrast, the use of stereology to get a 3D characterisation based on 2D SEM images was far easier, cheaper and faster. If the latter methodology is extensively used in the literature, its validity still needed to be checked with a direct 3D quantification as carried out here.

The average cell diameters obtained by the two methods, SEM and μ -CT, are consistent as can be observed in Fig. 10. Some discrepancies appear and can be due first to the low resolution of the tomograph which did not allow a correct segmentation of the cells (see e.g. T3P). Another difference was observed for the foams having the biggest cells, above 800 – 1000 μm . The values obtained from tomography were underestimated because the largest cells could not be taken into account in the analysis, leading to apparently normal cell size distributions instead of being log-normal. The corresponding samples were then no more representative of the whole material. Thus, in addition to its simplicity, stereology appears to be very efficient and more reliable in some cases.

However, it has been shown above that the cells are not perfect spheres. If we had to consider them as ellipsoids of revolution, their aspect ratios calculated from the sphericity indexes would range from 1.2 to 1.5. It was shown in [42] that for such ellipsoids the ratio D/\bar{L}_3 , which is equal to $3/2$ for spheres (see subsection 2.2.1.), becomes 1.55 and 1.51, respectively. These differences of ratios induced by the elongation of the cells are thus negligible with respect to the variability of the foams and the accuracy of the measurements. On the other hand, if the cells had to be described by tetrakaidecahedra, the coefficient calculated from the data of [13] would be equal to 1.78, which overestimates the cells' diameters. The tetrakaidecahedron is often used for modelling foams and is considered as a more elaborated way for describing the cells, but it does not account for the reality in the present case.

Looking at these results coming from stereology, one can wonder whether it is still relevant to characterize carbon foams with X-ray microtomography. As already stated in [43], if tomography indeed allows getting accurate results about the distributions of cells sizes, as well as their shapes and other parameters if the required resolution can be reached, it is

relatively costly and such extensive information may not be always required. Therefore, a simple methodology based on stereology for routine characterization can be preferred, the use of tomography being really relevant for a few samples only in order to check the validity of the data, obtain further information if needed, or perform 3D simulations of physical phenomena in real structures.

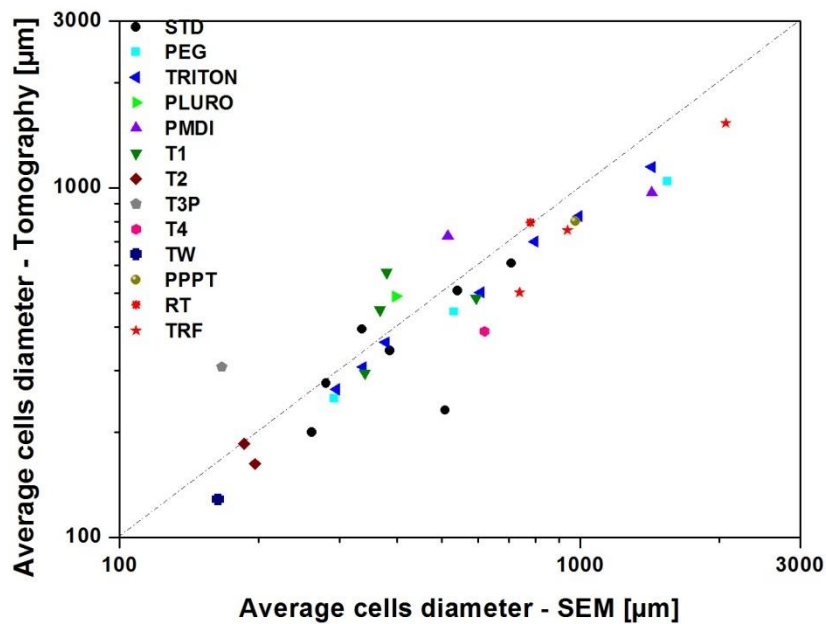


Fig. 10. Comparison of the average cell diameter determined with tomography (volume-weighted) and SEM.

4. Conclusion

A large number of cellular carbon foams with varied structures were produced, based on 14 types of formulations providing the possibility of modulating more or less independently bulk density on the one hand and cell size on the other hand. Each kind of carbon foam was prepared in the form of large and homogeneous blocks in which cutting off identical samples

for pyrolysis at 900°C followed by characterisation and further studies was possible. All these materials were cellular, except the formulation RT exhibiting a truly reticulated structure, i.e., free of cell walls.

When investigated through elemental analysis (chemical composition), helium pycnometry (skeletal density) and Raman spectroscopy (carbon texture), the different carbons obtained from the different formulations all proved to be extremely similar. For the further studies of the physical properties of these foams, we can therefore consider that only the porous structure changes from one sample to another. Moreover, as the skeletal density was always the same, this also means that all the carbon foams can be directly compared in terms of bulk density, here leading to the same conclusion as if compared in terms of relative density or porosity.

The morphology of the foams was essentially characterised through their bulk density and cell size. The average cell size was measured for all materials from SEM images, using a method based on cells counting along lines of known length and the use of relations coming from stereology. The relevance of this simple methodology was proved by comparison with an extensive X-Ray microtomography analysis. The latter allowed getting more detailed information, such as cells diameters distributions and shapes, but led to very similar average cell sizes and also demonstrated some limitations due to resolution and to samples sizes. We therefore showed that SEM studies are more relevant for our purposes.

The first step of this project, i.e., producing model carbon foams based on the same constitutive material but having different and controlled porous structures, is then successfully achieved. Many samples having different cell sizes at constant density, or different densities at constant cell size, were thus made available for a number of studies of physical properties. The corresponding work is presently in progress.

Acknowledgements

The authors gratefully acknowledge the financial support of the CPER 2007-2013 “Structuration du Pôle de Compétitivité Fibres Grand’Est” (Competitiveness Fibre Cluster), through local (Conseil Général des Vosges), regional (Région Lorraine), national (DRRT and FNADT) and European (FEDER) funds. The authors also thank the support of the Institut Universitaire de France, by which this project could be carried out.

References

- [1] Gibson LJ, Ashby MF. Cellular Solids: Structure and Properties. 2nd ed. Cambridge University Press; 1999.
- [2] Inagaki M, Qiu J, Guo Q. Carbon foam: preparation and application. Carbon 2015; 87: 128-52
- [3] Li X, Basso MC, Braghiroli FL, Fierro V, Pizzi A, Celzard A. Tailoring the structure of cellular vitreous carbon foams. Carbon 2012; 50(5):2026–36.
- [4] Tondi G, Fierro V, Pizzi A, Celzard A. Tannin-based carbon foams. Carbon 2009; 47(11): 1480–92.
- [5] Maheo L, Viot P, Bernard D, Chirazi A, Ceglia G, Schmitt V. et al. Elastic behavior of multi-scale, open-cell foams. Compos Part B Eng 2013; 44(1):172–83.
- [6] Dam CQ, Brezny R, Green DJ. Compressive behavior and deformation-mode map of an open cell alumina. J Mater Res 1990; 5(1):163–71.
- [7] Zhao W, Pizzi A, Fierro V, Du G, Celzard A. Effect of composition and processing parameters on the characteristics of tannin-based rigid foams. Part I: Cell structure. Mater Chem Phys 2010; 122(1):175–182.
- [8] Basso MC, Pizzi A, Celzard A. Influence of formulation on the dynamics of preparation of tannin-based foams. Ind Crops Prod 2013; 51:396–400.
- [9] Li X, Basso MC, Fierro V, Pizzi A, Celzard A. Chemical Modification of Tannin/Furanic Rigid Foams by Isocyanates and Polyurethanes. Maderas Cienc Tecnol 2012; 14(3):257-265.
- [10] Basso MC, Giovando S, Pizzi A, Celzard A, Fierro V. Tannin/furanic foams without blowing agents and formaldehyde. Ind Crops Prod 2013; 49:17–22.

- [11] Underwood EE. Quantitative stereology. Addison-Wesley Pub Co; 1970.
- [12] Underwood EE. Stereology, or the quantitative evaluation of microstructures. *J Microsc* 1969; 89(2):161–80.
- [13] Hilliard JE. The calculation of the mean caliper diameter of a body for use in the analysis of the number of particles per unit volume. Extended abstracts, 2nd International Congress for Stereology. Chicago (USA): The National Science Foundation and the International Society for Stereology, 1967; p. 211–5.
- [14] De Hoff RT. Transactions of the Metallurgical Society 230. AIME, 1964; p. 764.
- [15] Li X, Pizzi A, Lacoste C, Fierro V, Celzard A. Physical properties of tannin/furanic resin foamed with different blowing agents. *BioResources* 2013; 8(1):743–52.
- [16] Szczurek A, Fierro V, Pizzi A, Stauber M, Celzard A. Carbon meringues derived from flavonoid tannins. *Carbon* 2013; 65:214–27.
- [17] Martinez de Yuso A, Lagel MC, Pizzi A, Fierro V, Celzard A. Structure and properties of rigid foams derived from quebracho tannin. *Mater Des* 2014; 63:208–12.
- [18] Maire E. X-Ray Tomography Applied to the Characterization of Highly Porous Materials. *Annu Rev Mater Res* 2012; 42:163–78.
- [19] Youssef S. Etude par tomographie X et modélisation par éléments finis du comportement mécanique des mousses solides. Lyon France, Institut National des Sciences Appliquées de Lyon, PhD thesis, 2004.
- [20] Maire E, Buffiere JY, Salvo L, Blandin JJ, Ludwig W, Letang JM. On the application of X-ray microtomography in the field of materials science. *Adv Eng Mater* 2001; 3(8):539–46.

- [21] Maire E, Colombo P, Adrien J, Babout L, Biasetto L. Characterization of the morphology of cellular ceramics by 3D image processing of X-ray tomography. *J Eur Ceram Soc* 2007; 27(4):1973–81.
- [22] Loretz M. Caractérisation des propriétés thermiques de mousses céramiques et métalliques à partir d'analyses tomographiques aux rayons X. Lyon France, Institut National des Sciences Appliquées de Lyon, PhD thesis, 2008.
- [23] Trater AM, Alavi S, Rizvi SSH. Use of non-invasive X-ray microtomography for characterizing microstructure of extruded biopolymer foams. *Food Res Int* 2005; 38(6): 709–19.
- [24] Otsu N. A Threshold Selection Method from Gray-Level Histograms. *IEEE Trans Syst Man Cybern* 1979; 9(1):62–6.
- [25] Brun E. De l'imagerie 3D des structures à l'étude des mécanismes de transport en milieux cellulaires. Marseille France, University of Aix-Marseille, PhD thesis, 2009.
- [26] Shabalín IL. Ultra-High Temperature Materials I, Carbon (Graphene/Graphite) and Refractory Metals. Dordrecht: Springer Netherlands; 2014.
- [27] Tsaneva VN, Kwapinski W, Teng X and Glowacki. BA. Assessment of the structural evolution of carbons from microwave plasma natural gas reforming and biomass pyrolysis using Raman spectroscopy. *Carbon*, 2014; 80: 617–28.
- [28] Barros EB, Demir NS, Souza Filho AG, Jorio A, Dresselhaus G, Dresselhaus MS. Raman spectroscopy of graphitic foams. *Phys Rev B* 2005; 71:165422-1–5.
- [29] Soukup L, Gregora I, Jastrabik L, Konakova A. Raman spectra and electrical conductivity of glassy carbon. *Mat Sci Eng B* 1992;11:355-7.

- [30] Ray K III, McCreery RL. Spatially Resolved Raman Spectroscopy of Carbon Electrode Surfaces: Observations of Structural and Chemical Heterogeneity. *Anal Chem* 1997; 69: 4680-7.
- [31] Bukalov SS, Zubavichus YV, Leites LA, Sorokin AI, Kotosonov AS. Structural changes in industrial glassy carbon as a function of heat treatment temperature according to Raman spectroscopy and X-ray diffraction data. *Nanosystems: Phys Chem Math* 2014; 5(1):186–91.
- [32] Solopova NA, Dubrovinskaia N, Dubrovinsky L. Raman spectroscopy of glassy carbon up to 60GPa. *Appl Phys Lett* 2013; 102: 121909-1 – 4.
- [33] Nakamizo N, Kammereck, Walker PL Jr. Laser Raman studies on carbons. *Carbon* 1974; 12:259-67.
- [34] Saito R, Hofmann M, Dresselhaus G, Jorio A, Dresselhaus MS. Raman spectroscopy of graphene and carbon nanotubes. *Adv Phys* 2011; 60(3):413-550.
- [35] Beyssac O, Goffé B, Petitet JP, Froigneux E, Moreau M, Rouzaud JN. On the characterization of disordered and heterogeneous carbonaceous materials by Raman spectroscopy. *Spectrochim Acta A Mol Biomol Spectroscop* 2003; 59(10): 2267-76.
- [36] Ferrari AC, Robertson J. Raman spectroscopy of amorphous, nanostructured, diamond-like carbon, and nanodiamond. *Phil. Trans. R. Soc. Lond. A* 2004;362:2477–512.
- [37] Mallet-Ladeira P, Puech P, Toulouse C, Cazayous M, Ratel-Ramond N, Weisbecker P, et al. A Raman study to obtain crystallite size of carbon materials: A better alternative to the Tuinstra–Koenig law. *Carbon* 2014; 80: 629-39.

- [38] Limpert E, Stahel WA, Abbt M. Log-normal Distributions across the Sciences. *BioScience* 2001; 51(5):341–52.
- [39] Picandet V. Characterization of Plant-based aggregates. In: Amziane S, Arnaud L, editors. *Bio-Aggreg -Based Build Mater Appl Hemp Concr*, ISTE, John Wiley & Sons; 2013 p. 27–74.
- [40] Saltikov SA. The determination of the size distribution of particles in an opaque material from a measurement of the size distribution of their sections. Extended abstracts, 2nd International Congress for Stereology. Chicago (USA): The National Science Foundation and the International Society for Stereology, 1967; p.163-74.
- [41] Goel SK, Beckman EJ. Generation of microcellular polymeric foams using supercritical carbon dioxide. I: Effect of pressure and temperature on nucleation. *Polym Eng Sci* 1994; 34(14):1137–47.
- [42] Sahagian DL, Proussevitch AA. 3D particle size distributions from 2D observations: stereology for natural applications. *J Volcanol Geotherm Res* 1998; 84:173–96.
- [43] Exner HE. Stereology and 3D microscopy: useful alternatives or competitors in the quantitative analysis of microstructures? *Image Anal Stereol* 2004; 23:73-82.

Caption of Tables

Table 1: Formulations of the different types of foams.

Table 2: Elemental analysis of carbon foams. All elements are expressed in wt. %.

Table 3: Adjustable coefficients of the power law fits to the data of Fig. 7.

Caption of Figures

Figure 1: Mould (left) used for the preparation of tannin-based foams (right).

Figure 2: SEM pictures (secondary electrons detector) of vitreous carbon foams prepared from different formulations (see text): (a) type STD ($\times 30$) with densities of 0.043 (top) and 0.111 g cm⁻³ (bottom); (b) type PMDI ($\times 30$) with densities of 0.091 (top) and 0.188 g cm⁻³ (bottom); (c) type T1 ($\times 30$) with densities of 0.021 (top) and 0.033 g cm⁻³ (bottom); (d) type T2 with densities of 0.050 ($\times 500$, top) and 0.129 g cm⁻³ ($\times 30$, bottom); (e) types T3P ($\times 500$, top) and TW ($\times 30$, bottom) with densities of 0.036 and 0.044 g cm⁻³, respectively; (f) types PPPT ($\times 30$, top) and RT ($\times 30$, bottom) with densities of 0.094 and 0.043 g cm⁻³, respectively.

Figure 3: Changes of bulk density of cellular carbon foams as a function of the amount of blowing agent (diethyl ether) in the initial formulation. Power law fits to the data of each type of formulation are shown in the inset.

Figure 4: Thermogravimetric analysis of an STD organic foam and simultaneous mass spectrometer analysis of the emission of CO, O and CO₂ as a function of time. After the pyrolysis up to 900°C, one 4h-long isothermal segment of and two other cycles of heating and cooling between 200 and 900°C were performed. The data from the detector of the mass spectrometer are in Ampere (no calibration).

Figure 5: Comparison of the bulk densities of foams made from different formulations, before and after pyrolysis.

Figure 6: Raman spectra at 532 nm of most carbon foams presented in this study: (a) full spectra; (b) zoom on the 1st order part; (c) positions of D and G bands as a function of D/G intensity ratio.

Figure 7: Average cell diameter determined from SEM pictures as a function of bulk density. The straight lines are power law fits such as $D = A\rho^x$ to the data sets of each type of formulation.

Figure 8: Number-weighted (a) and volume-weighted (b) distributions of equivalent cells diameters of an STD foam sample of bulk density 0.065 g cm^{-3} . The curves corresponding to the cumulative percentages and to log-normal fits of the distributions are also shown.

Figure 9: (a) Polydispersity indexes of number-weighted and volume-weighted distributions; (b) volume-weighted average cell diameters, with their 68% confidence intervals, as a function of bulk density; (c) sphericity indexes as a function of average cell diameter.

Figure 10: Comparison of the average cell diameter determined with tomography (volume-weighted) and SEM.